Cell Reports
Physical Science

CellPress
OPEN ACCESS

Article

Stretchable and conductive fibers fabricated by a continuous method for wearable devices

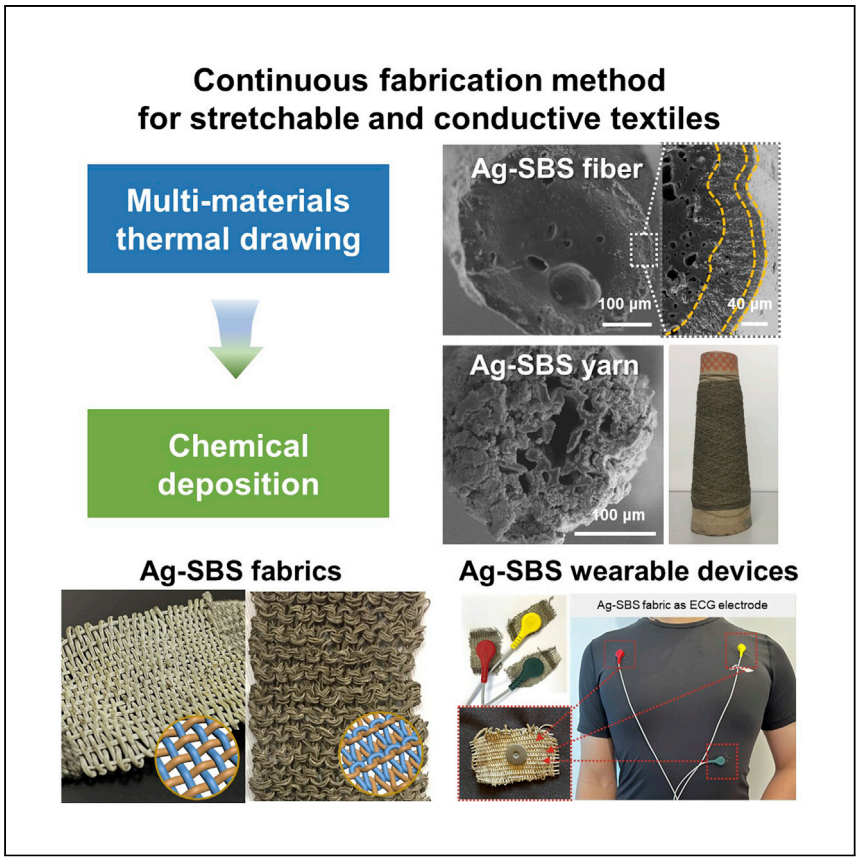

Ma et al. develop a continuous approach for fabricating stretchable and conductive fibers, which are suitable for being twisted into textile yarns, woven and knitted into textile fabrics, or braided and stitched onto textile structures. These textiles can be assembled into breathable and washable devices for wearable electronic applications.

Zhijun Ma, Qiyao Huang, Ningjing Zhou, Qiuna Zhuang, Sze-Wing Ng, Zijian Zheng

tczzheng@polyu.edu.hk

Highlights

A continuous approach is developed for stretchable and conductive fibers

The mechanical and electrical properties of the fibers can be facilely tailored

The fibers can be processed into fabrics for breathable and washable devices

Ma et al., Cell Reports Physical Science 4, 101300
March 15, 2023
https://doi.org/10.1016/j.xcrp.2023.101300

Cell Reports
Physical Science

CellPress
OPEN ACCESS

Article

Stretchable and conductive fibers fabricated by a continuous method for wearable devices

Zhijun Ma,[1,2,3,7] Qiyao Huang,[1,4,7] Ningjing Zhou,[3] Qiuna Zhuang,[1] Sze-Wing Ng,[1] and Zijian Zheng[1,4,5,6,8,*]

SUMMARY

Stretchable and conductive fibers are building blocks for the development of a wide range of wearable and stretchable electronics owing to their small size, light weight, omnidirectional pliability and elasticity, and outstanding integration ability. Despite a large number of reports in the past decade, there is a lack of a continuous and scalable approach to manufacturing stretchable and conductive fibers with sufficient strength, elasticity, conductivity, and durability. Here we report a high-throughput fabrication method based on continuous multimaterial thermal drawing and chemical deposition processes to produce highly stretchable and conductive fibers, which are suitable for being twisted into textile yarns, woven and knitted into textile fabrics, or braided and stitched onto textile structures. We demonstrate the assembly of these stretchable and conductive fibers into breathable, machine-washable, and wearable devices for body motion detection, electrothermal therapy, and electrocardiograph signal detection.

INTRODUCTION

Stretchable electronics exhibit enormous application possibilities in wearable electronics, soft robotics, medical implants, and biological actuators for the future.[1–4] In the past decades, the majority of stretchable electronics have been developed based on thin-film structure, e.g., electronic devices and systems are fabricated on elastic thin-film substrates.[2] In recent years, fiber-based stretchable electronic devices have received remarkable attention from academia and industry. Compared with thin-film-based devices, fiber-based stretchable electronics can possess higher compliance to the curvilinear surface of the human body, greater adaptability to the frequent deformations of the body during usage, and superior breathability for air, moisture, and body liquids.[5–8] In particular, when functional fibers are used as building blocks, they are easy to incorporate into yarns, fabrics, and garments, enabling the imperceptible integration of electronics into wearable forms.[9,10] To date, a series of fiber-shaped stretchable electronic devices, such as stretchable sensors,[11–15] supercapacitors and batteries,[16–19] nanogenerators,[20–22] and solar cells,[23,24] has been demonstrated. Among all these demonstrations, the robust preparation of highly conductive and stretchable fibers, which act as conducting interconnectors, electrodes, and antennas, is an indispensable yet challenging step.[25] Especially, it is highly desirable to fabricate them in a continuous and high-throughput manner and to assemble them into superstructures that are easier to integrate into different wearable applications.

Generally, there are four strategies for the fabrication of stretchable conductive fibers. In the first strategy, flexible conductive materials, such as metal nanowires,

[1]Laboratory for Advanced Interfacial Materials and Devices, School of Fashion and Textiles, The Hong Kong Polytechnic University, Hong Kong SAR 999077, China

[2]Research Center for Humanoid Sensing, Research Institute of Intelligent Sensing, Zhejiang Lab, Hangzhou 311121, China

[3]State Key Laboratory of Luminescent Materials & Devices, Guangdong Engineering Technology Research and Development Center of Special Optical Fiber Materials and Devices, Guangdong Provincial Key Laboratory of Fiber Laser Materials and Applied Techniques, School of Materials Science and Engineering, South China University of Technology, Guangzhou 510641, China

[4]Research Institute for Intelligent Wearable Systems, The Hong Kong Polytechnic University, Hong Kong SAR 999077, China

[5]Department of Applied Biology and Chemical Technology, The Hong Kong Polytechnic University, Hong Kong SAR 999077, China

[6]Research Institute for Smart Energy, The Hong Kong Polytechnic University, Hong Kong SAR 999077, China

[7]These authors contributed equally

[8]Lead contact

*Correspondence: tczzheng@polyu.edu.hk

https://doi.org/10.1016/j.xcrp.2023.101300

carbon-based materials, conductive polymers, and continuous conductive threads, are wrapped around the surface of a non-conductive elastic fiber. Buckles of the conductive coating can be formed by prestretching the elastomer substrate and subsequently releasing the strain on the fiber, which can substantially enhance the stretchability and stability of the fibers.[13,26–28] Although this approach can achieve structurally stretchable fibers with high conductivity and electrical stability, inevitable delamination between the conductive sheath and the substrate will seriously degrade the performance of the fibers. Meanwhile, the prestretch method is difficult to implement on a large scale or to assemble into different superstructures. In the second strategy, bundles of carbon nanomaterials, typically carbon nanotubes and graphene, are directly spun into stretchable conductive fibers. By further twisting the carbon fibers into helical structures and combining with an elastomer, the stretchability of the fibers can be remarkably enhanced.[29–32] The excellent chemical stability and high specific surface area make the carbon-based stretchable fibers ideal as electrodes for constructing high-performance one-dimensional energy conversion or storage devices, such as solar cells, batteries. and supercapacitors. However, the relatively high material cost and the low fabrication efficiency make it challenging for this strategy to perform large-scale production. In the third strategy, liquid conductors (typically liquid metal and ionic liquid) are sealed in channels of elastomer fibers by injection to form core-sheath fibers.[33–35] Both super stretchability and high conductivity can be achieved by this strategy, but serious caution should be taken to prevent the leakage of liquid conductors. In the fourth strategy, stretchable conductive fibers are fabricated via spinning approaches. Conductive materials, typically metal particles/nanowires, carbon nanotubes, graphene, and liquid metal droplets, are dispersed into the matrix of elastomer materials and then spun into stretchable conductive fibers.[11,36–38] This strategy is promising for the continuous fabrication of stretchable conductive fibers with highly tailorable mechanical and electrical properties. Nevertheless, the massive use of solvents during the spinning process is known to be environmentally unfriendly. The removal of residue solvent is also a tedious process that may easily lead to non-uniformity and low strength of the fibers.

On the other hand, multimaterial thermal drawing (MMTD), which was initially used for the fabrication of composite optical fibers, is a powerful method for large-scale continuous fabrication of fibers.[39–42] MMTD makes use of a multimaterial preform that could be drawn into fibers under controlled thermal conditions. In this way, fibers incorporating multicomponents of disparate materials with predesigned geometries can be directly and continuously formed without the need for a solvent.[43] Therefore, MMTD has been regarded as an environmentally friendly manufacturing approach.[44] Meanwhile, in a typical MMTD process, geometrical properties of the preform can be replicated by the drawn fibers with high fidelity, which is important for tuning the performance of the fibers. Therefore, the MMTD method can precisely control the nano- to microscale geometrical properties of fiber by tailoring the macroscale geometrical properties of the preform. It has been recently demonstrated that the synchronous injection of liquid metal into the prescribed hollow elastomer preform could lead to the thermal drawing of core-shell-structured multimaterial fibers with promising stretchability and conductivity.[34,45–47] However, such metal-in-rubber core-shell fiber design is not suitable for electrodes for device applications due to the difficulty in contacting the conductive metal core with active materials. While dip-coating of conductive materials around the as-made stretchable fiber could address the contact problem,[48] it is challenging to simultaneously enable high stretchability and conductivity in the fibers.

Chemical deposition is a versatile technology for the fabrication of soft-metal circuits and electrodes.[49–51] Compared with physical technologies such as vacuum thermal deposition, the chemical deposition technologies are advantageous in many aspects, such as high compatibility with various soft substrates, scalability for mass production, and low cost. Specifically, by using thermoplastic elastomers (TPEs) containing unsaturated or aromatic hydrocarbons as the substrate and an alcoholic solution of silver trifluoroacetate (AgTFA) as the growing medium, followed by an *in situ* reduction process, stretchable conductors with super elasticity, high conductivity, and stability have been prepared by chemical deposition.[36,52,53] The chemical deposition is also more compatible with the wet chemical approaches for functional finishing in the current textile industry.

In this work, we demonstrate for the first time a versatile and continuous approach for fabricating high-performance stretchable and conductive fibers, yarns, and textiles based on MMTD and chemical deposition. A preform composed of a TPE core (i.e., poly(styrene-block-butadiene-block-styrene) [SBS]) and a thermoplastic polymer (i.e., poly(methyl methacrylate) [PMMA]) cladding was designed and then thermally drawn into a continuous microscale fiber. Subsequent removal of the cladding and chemical deposition of the silver nanoparticles (AgNPs) were conducted in a roll-to-roll manner to further impart the fiber with stretchability and electrical conductivity. Benefiting from the elasticity of the elastomeric fiber core and the high electrical conductivity of the AgNP coating, the AgNP-loaded SBS fibers (denoted as Ag-SBS fibers) possess superior electrical conductivity (up to ~4,400 S cm^{-1}) and stretchability (>1,500% strain). Through the geometrical design of the preform for the MMTD process, this continuous fabrication approach also allows the scalable production of stretchable multifilament yarns with tunable yarn configurations and electrical conductivity. Importantly, as-made fibers and yarns are strong enough to be integrated into various textile fabrics and garments through conventional textile manufacturing processes such as weaving, knitting, and braiding. They can serve as the breathable building blocks of textile-based electrodes for body motion detection, electrocardiograph (ECG) signal collection, and electrothermal therapy.

RESULTS AND DISCUSSION

Continuous fabrication of stretchable and conductive AgNP-loaded SBS fibers

Figure 1 illustrates the continuous fabrication of stretchable and conductive Ag-SBS fiber. First, the MMTD method was adopted to produce an elastic fiber that could act as the structural core for the conductive fiber (Figure 1A). In this method, a multimaterial preform composed of an elastomeric SBS core and a PMMA cladding (denoted as PMMA@SBS) (Figure 1B) was thermally drawn into a continuous core-sheath-structured fiber (denoted as PMMA@SBS fiber) on a fiber-drawing tower (Figure S1A). Such an MMTD method allows reducing the diameter of the core-cladding preform by more than 200 times, meanwhile producing thousands of meters of core-sheath-structured fiber in a typical single drawing process (Figure 1C). Due to the higher melting temperature of PMMA (Figure S1B) compared with that of SBS (Figure S1C), PMMA was selected as the cladding of the elastomeric SBS core to promise the conformal elongation of both the core and the cladding of the PMMA@SBS preform when heated (Figures 1C and 1D) and to avoid the thermal decomposition of the SBS fiber core during the thermal drawing process. In addition, the PMMA sheath can be selectively removed by the post-dissolution process without affecting the properties of the SBS fiber core. After the MMTD process, the drawn PMMA@SBS fiber was soaked in a bath of glacial acetic acid to remove the PMMA sheath, through which an SBS fiber (diameter ~360 μm) could be obtained

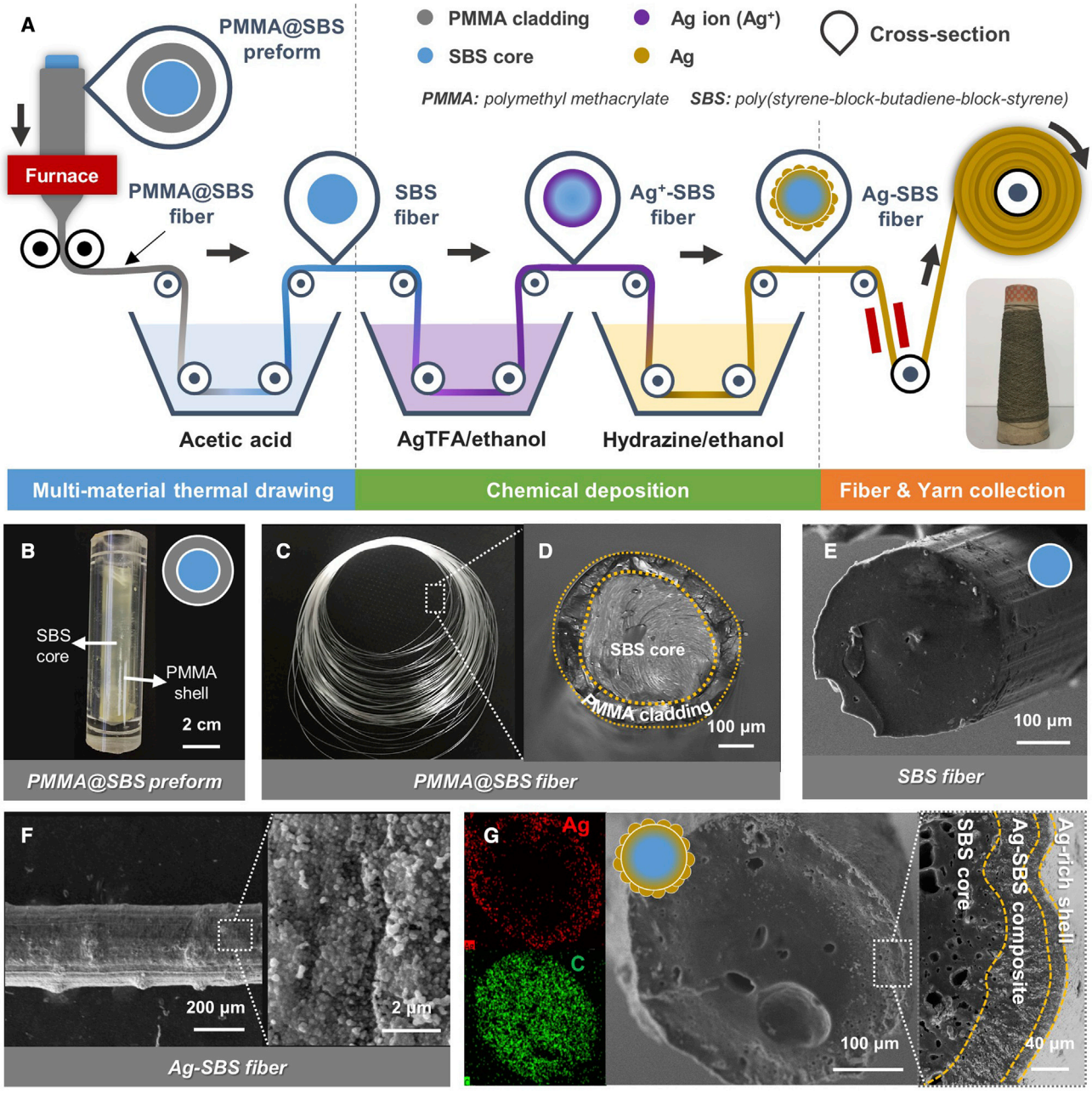

Figure 1. Continuous fabrication of stretchable and conductive Ag-SBS fibers

(A) Schematic illustration of the fabrication process of Ag-SBS fibers.

(B) Digital image of the PMMA@SBS preform prepared for multimaterial thermal drawing.

(C) Digital image of the PMMA@SBS fiber thermally drawn from the PMMA@SBS preform.

(D) Optical image of the cross section of the PMMA@SBS fiber.

(E) Cross-sectional SEM image of the SBS fiber after the dissolution of PMMA cladding.

(F) SEM images showing the Ag-SBS fiber (left) and the Ag coating on the fiber surface (right).

(G) Cross-sectional SEM images and the corresponding EDS mapping showing the distribution of the loaded Ag in the SBS fiber.

(Figure 1E). To impart electrical conductivity, the SBS fiber went through the chemical deposition process, in which the fiber was continuously soaked in an ethanol solution of AgTFA ($AgCF_3COO_2$) to absorb Ag precursors and then soaked in another ethanolic solution of hydrazine (N_2H_4) to reduce the absorbed Ag ions into AgNPs.

Due to an ion-dipole interaction between the TFA anions (CF_3OO^-) and the hydroxyl groups (–OH) of the ethanol solvent,[52] Ag precursors could be massively absorbed into the SBS fiber in the absorption step. Subsequent conversion of Ag precursors into AgNPs could complete with the preparation of the Ag-SBS fiber. Since both the absorption and the reduction steps were performed in a continuous roll-to-roll fabrication manner, one could obtain the Ag-SBS fiber on a kilometer scale (inset in Figure 1A).

Scanning electron microscope (SEM) images of the Ag-SBS fibers reveal that AgNPs were densely loaded onto the surface of the fiber (Figure 1F). In addition, a substantial amount of AgNPs were embedded inside the SBS fiber (Figure 1G). This is because the Ag precursors diffused toward the center of the fiber during the absorption step of Ag precursors, resulting in the formation of an AgNP coating layer that was not only around the fiber surface as a rigid Ag-rich shell but also in the fiber matrix as an AgNP-SBS composite. The distribution of the AgNPs along the fiber surface and inside the fiber was identified in the energy-dispersive X-ray spectroscopy (EDS) mapping of the cross section of the Ag-SBS fiber (Figure 1G).

Electrical and mechanical properties of Ag-SBS fibers

The MMTD method used here can flexibly adjust the diameter of the SBS fiber by tuning the drawing speed, through which electrical and mechanical properties of the Ag-SBS fibers can be varied. In general, the diameter of the SBS fiber decreased with the increase in fiber drawing speed. When the drawing speed was set as 3 mm s^{-1}, the diameter of the Ag-SBS fiber was ~630 μm. Further increasing the drawing speed to 10 mm s^{-1} and even 80 mm s^{-1} could lead to finer Ag-SBS fibers with diameters of 390 and 110 μm, respectively. Under the same loading conditions of AgNPs, reducing diameter could effectively increase the absorption efficiency of the Ag precursor, which was beneficial for forming a higher amount of AgNPs in the fiber and thus enabling a higher electrical conductivity. As summarized in Figure 2A, SBS fibers with 110 μm diameter exhibited the highest AgNP uptake of 66% compared with those with larger diameters, demonstrating a 295-fold increase in initial electrical conductivity (1,300 S cm^{-1}) compared with the Ag-SBS fiber with 630 μm diameter (4.4 S cm^{-1}). More importantly, higher AgNP uptake could enable a denser electrical connection in the fiber, leading to the enhancement of electrical stretchability of the fiber. The resistance of 110-μm-diameter Ag-SBS fibers gradually increased by only 90 times at 25% strain, suggesting that a dense distribution of AgNPs was still preserved in such a finer fiber matrix under a large strain. In contrast, coarser Ag-SBS with diameters of 630 μm showed a rapid resistance change at a strain of less than 25% (Figure S2A). Such a sharp increase in resistance revealed the disconnection of the AgNP network in both the Ag shell and the AgNP-SBS composite region, which resulted from the insufficient percolation of AgNPs in the fiber matrix (Figure S2B). In terms of the mechanical properties, finer Ag-SBS fibers show a significant increase in tensile strength (37.7 MPa) with a slight decrease in breaking strain (1,150%), which may be ascribed to the enhanced mass ratio of AgNPs and orientation degree of the SBS molecules caused by the accelerated fiber drawing speed (Figures S2C and S3).[54–56]

The electrical and mechanical properties of the Ag-SBS fibers could also vary with the number of loading cycles for AgNPs. By repeating the chemical deposition steps (i.e., absorption of and reduction of Ag precursor) up to seven times, the initial electrical conductivity of the Ag-SBS fiber (diameter 390 μm) could be enhanced from 22 S cm^{-1} with only one-time loading of AgNPs to 4,415 S cm^{-1} (Figure 2B). Such

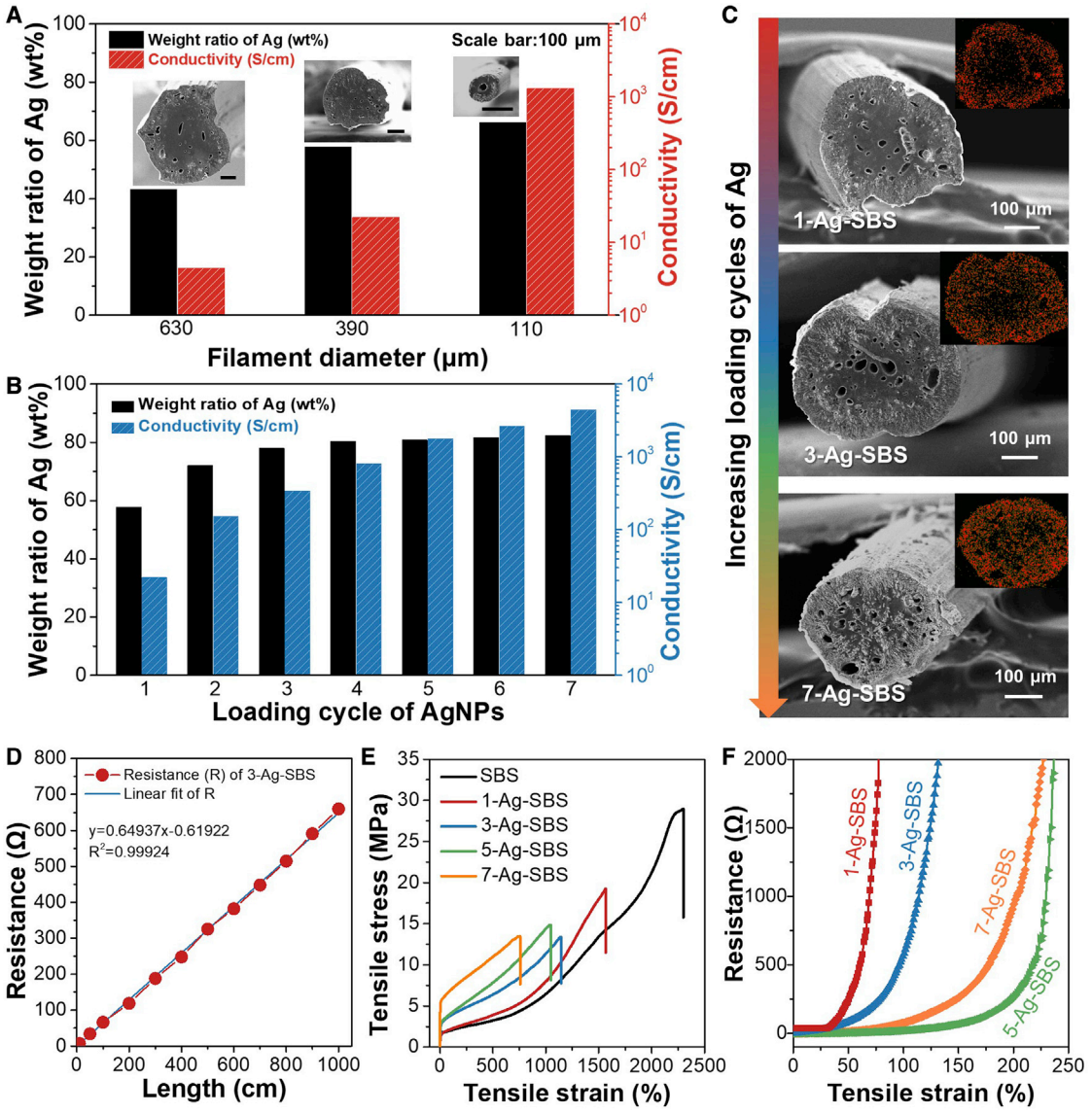

Figure 2. Mechanical and electrical properties of Ag-SBS with different fiber diameters and chemical deposition parameters

(A) Weight ratio of AgNPs and the corresponding conductivity of Ag-SBS fibers with different fiber diameters (loading cycle of AgNPs: 1).

(B) Weight ratio of AgNPs and the corresponding conductivity of Ag-SBS fibers with different loading cycles of AgNPs.

(C) Cross-sectional SEM images and corresponding EDS mapping of Ag-SBS fibers made by different loading cycles of AgNPs.

(D) Resistance of Ag-SBS (loading cycle of AgNPs: 3) as a function of fiber length.

(E) Tensile stress-strain curves of Ag-SBS fibers made by different loading cycles of AgNPs.

(F) Resistance of Ag-SBS fibers made by different loading cycles of AgNPs with increasing strain.

repetitive steps could increase the loading amount of AgNPs anchoring both around and inside the SBS matrix, leading to the formation of denser electrical connections of AgNPs in the fiber core (Figure 2C). Note that the repeated chemical deposition process of AgNPs onto the SBS fiber was carried out in a roll-to-roll manner so that the uniform uptake of AgNPs along with the fiber length could be ensured. The resistance value of the Ag-SBS fiber with three cycles of AgNP loading (denoted as 3-Ag-SBS) linearly increased as the length of fiber increased (Figure 2D), further demonstrating the consistency in the scalable production of Ag-SBS fibers via MMTD and roll-to-roll chemical deposition process.

Although the electrical conductivity of the Ag-SBS fiber was significantly enhanced by the repeated chemical deposition of AgNPs, the breaking stress and strain gradually decreased (Figure 2E). This is because a higher weight ratio of AgNPs embedded in the fiber significantly affects the elastic properties of the composite between metal particles and elastomers.[11] Nevertheless, the mechanical stretchability of these conductive fibers was still sufficient to satisfy the stretching range of practical applications in wearable electronics. The electrical stretchability of the Ag-SBS fibers with different loading cycles of AgNPs was then evaluated. To some extent, the maximum strain at which the fiber retained its electrical conductivity increased with the increased loading cycles of AgNPs, which could be ascribed to the enhanced conductive connection of AgNPs in the fiber matrix. When the loading cycles of AgNPs reached 5, the Ag-SBS fiber did not exhibit a rapid increase in the electrical resistance until it was stretched to more than 200% strain. Interestingly, further increasing the loading cycles to 7 did not show the enhancement of the electrical stretchability, in that the resistance of 7-Ag-SBS fiber increased abruptly with strain above 150%. This might be attributed to the situation in which excessive AgNP aggregation at the outmost fiber surface cracked at the large stretching stain, so that the electrical conductance between conductive fillers (i.e., AgNPs in Ag-rich shell and the AgNP-SBS composite regions) was hindered (Figure 2F).

Fabrication and performance of Ag-SBS multifilament yarns

The use of the MMTD approach can not only realize the continuous fabrication of an Ag-SBS monofilament, demonstrated above, but can also enable the one-step formation of conductive multifilament yarn (i.e., a continuous fiber bundle composed of more than one filament). Meanwhile, a twist could also be introduced into the multifilament yarn by rotating the preform during the fiber-drawing process. In a typical fabrication process, PMMA@SBS fiber drawn from the PMMA@SBS preform (illustrated in Figure 1A) was cut into short sticks and inserted into another PMMA tube to form a core-cladding PMMA@(PMMA@SBS) preform. Such a PMMA@(PMMA@SBS) preform with a core of multiple PMMA@SBS fibers was then subjected to a second thermal drawing process to form a PMMA@(PMMA@SBS) fiber (Figure 3Ai), followed by the removal of the PMMA cladding to obtain a yarn with multiple SBS fibers (Figure 3Aii). During the second drawing, the rotation of the PMMA@(PMMA@SBS) preform could enable a twist configuration to the as-drawn SBS multifilament yarns. Subsequent chemical deposition steps enabled the formation of a conductive yarn with multiple Ag-SBS fibers (i.e., Ag-SBS multifilament yarn, Figure 3Aiii). In this process, the number of Ag-SBS fibers in such a conductive yarn could be flexibly changed by adjusting the number of PMMA@SBS sticks that were inserted into the PMMA tube, while the twist level (i.e., the number of twists in 1 cm of yarn [tpcm]) could be tuned by changing the rotating speed of the preform.

As a proof of concept, we successfully demonstrated the continuous fabrication of stretchable and conductive Ag-SBS multifilament yarns with 87 filaments (denoted as 87F-Ag-SBS yarn) and tunable twist levels (Figures 3B–3D). Here, three cycles of the chemical deposition step were performed for all the yarn samples. We found that multifilament yarns exhibited higher electrical conductivity (~790 S cm^{-1} for 87F-Ag-SBS yarns) than monofilament yarn (341 S cm^{-1}) (Figure 3A). This could be attributed to the larger surface area for AgNP loading in the multifilament yarns. Under the condition of the same yarn diameter, yarn with more filaments would have finer filaments, which could significantly increase the specific surface area of the yarn and thus accelerate the loading efficiency of AgNPs (Figure S4). In addition, the presence of voids in the multifilament yarn could facilitate the formation of

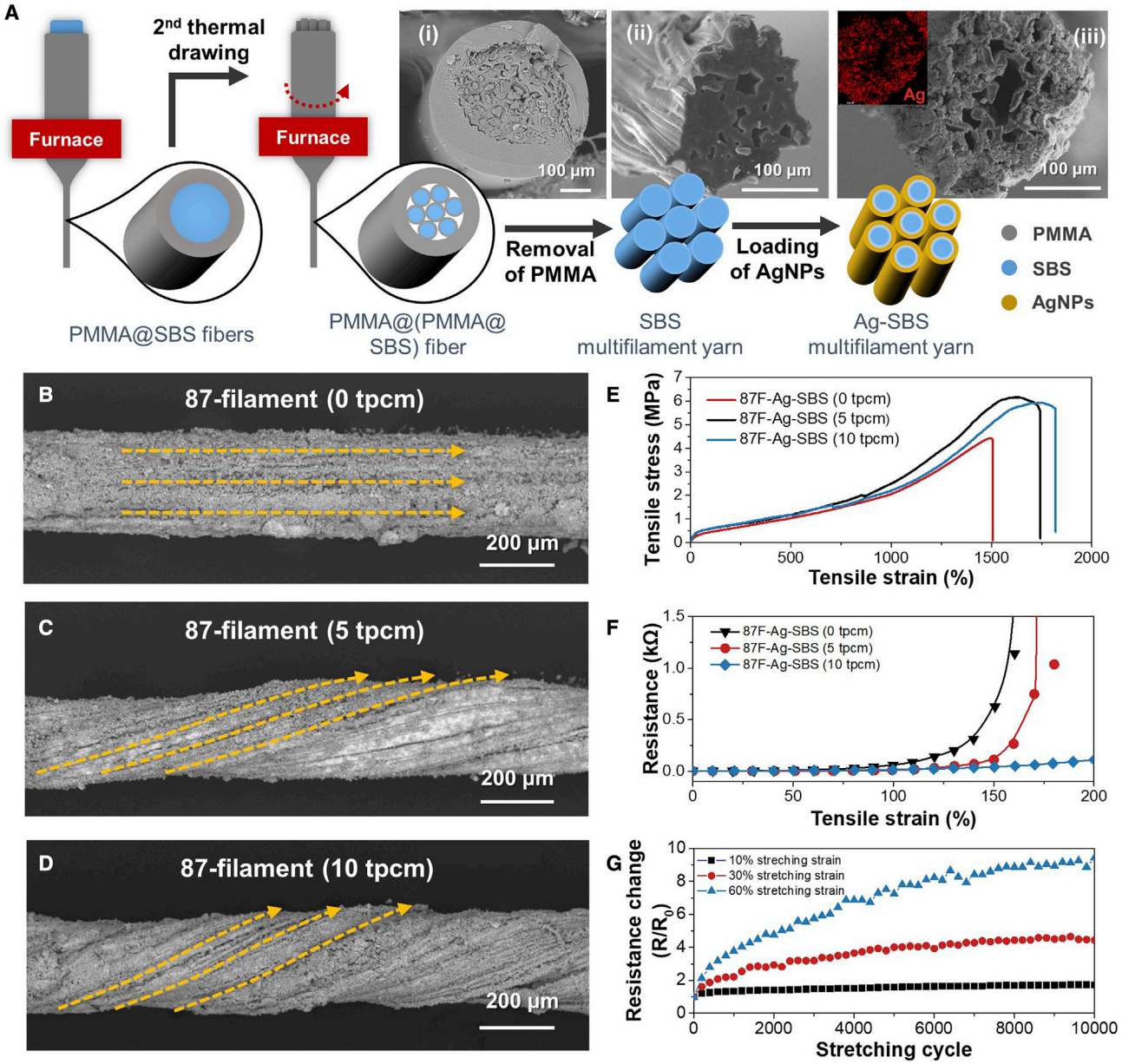

Figure 3. Fabrication and characterization of Ag-SBS multifilament yarns

All the yarn samples were treated with three cycles of chemical deposition of AgNPs.

(A) Schematic illustration showing the fabrication process of Ag-SBS multifilament yarns. Insets are the cross-sectional images of the PMMA@(PMMA@SBS) fiber (i), SBS multifilament yarn (ii), and Ag-SBS multifilament yarn (iii).

(B) SEM image of the Ag-SBS yarn with 87 filaments and without twist.

(C) SEM image of the Ag-SBS yarn with 87 filaments and with 5 twists in 1 cm (5 tpcm).

(D) SEM image of the Ag-SBS yarn with 87 filaments and with 10 twists in 1 cm (10 tpcm).

(E) Tensile stress-strain curves of Ag-SBS multifilament yarns made by different twist levels.

(F) Resistance of Ag-SBS multifilament yarn made by different twist levels.

(G) Change in resistance of the resistance of Ag-SBS multifilament yarns toward the repeated stretching cycles under different strains.

AgNPs inside the yarn structure (Figure 3Aiii), resulting in a larger amount of conductive contact within the fiber bundles to achieve higher electrical conductivity. We also found that twisting of the fiber bundle leads to a change in yarn structure and, consequently, to changes in the mechanical properties of the multifilament

yarn. The 87F-Ag-SBS yarn with a twist level of 5 tpcm showed ~1.08 times higher breaking strain (1,620%) and ~1.4 times higher tensile strength (6.2 MPa) than that without twist (1,500% breaking strain; 4.4 MPa breaking stress). Further increasing the twist level to 10 tpcm could enable an even higher break strain of 1,750% (Figure 3E). A proper amount of twist could introduce lateral compression into the fibers when the yarn was subjected to tensile stress, resulting in an increase in friction between individual fibers. This could explain the strength and strain improvements for twisted multifilaments compared with the yarn without twist.[57,58]

In addition, multifilaments became more engaged with one another with the increase in twist number in the fiber bundle, and thus the resistance changes against stretching tended to diminish. The resistance of the multifilament yarn with a twist level of 10 tpcm increased by only 75 times at 200%, while yarns with a lower twist and without twist had a sharp resistance increase below 150% (Figure 3F). We further investigated the endurance of the Ag-SBS multifilament yarn to the repeating mechanical deformations. After 10,000 cycles of stretching under the strain of 10%, the resistance of the twisted 87F-Ag-SBS yarns (5 tpcm) increased by only 1.73 times. Even though the strain was increased to 60%, the resistance of the yarn increased by as low as 9.44 times after 10,000 cycles of stretching (Figure 3G). The above results demonstrated the versatility of the continuous fabrication strategy based on MMTD and chemical deposition processes in tuning the geometrical structures (number of filaments in the fiber bundle and twist level) of filament yarns, which is of significant importance for simultaneously achieving superior mechanical and electrical properties of stretchable fiber conductors.

Fabrics and washable wearable devices made with Ag-SBS yarns

The Ag-SBS yarns possessed outstanding mechanical properties that well matched the requirements of conventional textile technologies. As such, one could develop a variety of conductive textiles via different textile fabrication methods, such as plain weave by weaving technology, plain knits via knitting technology, and ropes via the braiding method (Figures 4A–4C). It is worth noting that the textile structure further enhanced the stretchability of the Ag-SBS textiles. The Ag-SBS knitted fabric exhibited the best performance in stretchability (maximum strain 240%) and conductivity (resistance change [R/R_0] 20 at 200% strain and 65 at 240%) (Figure 4D). In addition, we demonstrated the feasibility of implementing a conventional weaving loom to create Ag-SBS fabric with pattern construction. Ag-SBS yarns serving as the weft yarns could be inserted into the warp shed to create a twill weave (Figure 4E). Note that these textile structures were all formed with fibrous materials via conventional textile technologies so that they could exhibit outstanding air permeability (<0.8 kPa $s \cdot m^{-1}$) and moisture permeability (>540 g m^{-2} day^{-1}) that were comparable to those of commercially available fabrics (Figure 4F). These results demonstrated the great promise of Ag-SBS yarns in being integrated into daily clothes for wearable health-care applications without affecting wearing comfort.

The scalable fabrication of Ag-SBS filaments and yarns enables the highly versatile development of fabric electrodes and devices for diverse wearable applications, including sensing and actuation. As a proof of concept, we demonstrated the application of Ag-SBS yarns and fabrics in smart gloves, heating textiles, and ECG electrode fabrics respectively for body motion detection, electrothermal therapy, and health-care monitoring. In the first demonstration, a smart glove was made by attaching the Ag-SBS yarns to the finger positions of a glove (Figure 5A). When the glove was worn, finger movements could lead to a resistance change in the

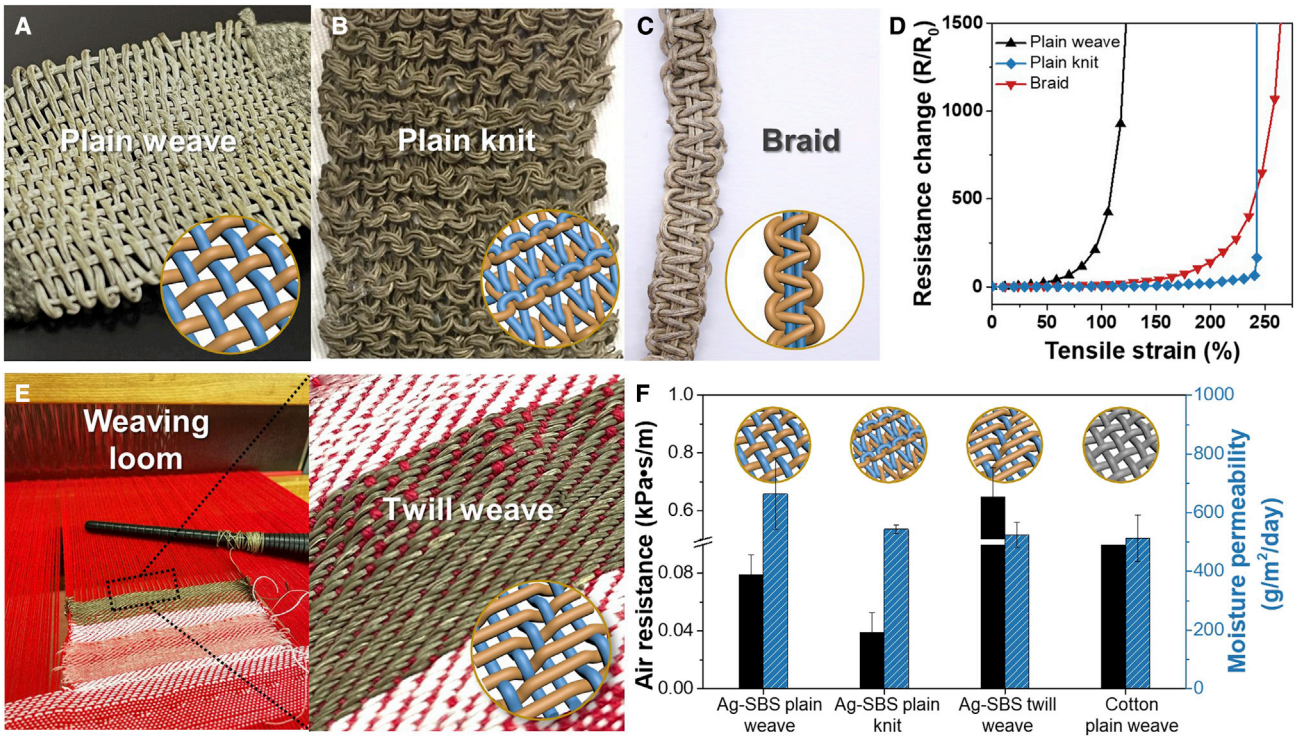

Figure 4. Fabrication and characterization of Ag-SBS textiles

All Ag-SBS yarns were treated with three cycles of chemical deposition of AgNPs.

(A–C) Digital images showing the structures of Ag-SBS plain weave (A), Ag-SBS plain knit (B), and Ag-SBS braid (C). Insets are schematic illustrations showing the corresponding textile structures.

(D) Resistance change in the Ag-SBS textiles made with different textile technologies with increase in stretching strain.

(E) Digital images showing the conventional weaving loom (left) that could be used to form Ag-SBS twill woven fabric (right). Inset is a schematic illustration showing the twill weave structure.

(F) Air resistance and moisture permeability of Ag-SBS textiles made by different textile technologies in comparison with conventional cotton plain-woven fabric. Error bars represent the standard deviation (SD).

corresponding stretchable and conductive yarns of the glove. As such, the glove can be applied to the identification of various hand gestures (Figure 5B). In the second demonstration, the Ag-SBS fabric functioned as an electrothermal heater, which could respond sensitively and quickly to the applied voltage and could stably perform its electrothermal therapy function at both flat and bent states during wearing (Figures 5C and 5D). The surface temperature of the heater (size 4 × 5 cm^2) could reach ~41°C within 100 s under the applied voltage of 0.8 V with a heating efficiency of ~0.2°C V^{-1} s^{-1}. At a steady voltage of 0.8 V, the output temperature changed only by less than 10% when the fabric device was stretched to 30% (Figure 5E). The fabric heater also performed promising device stability upon heating cycles (Figure 5F).

Last, but not least, permeable woven fabrics made by interlacing Ag-SBS yarns could directly serve as the electrodes for collecting ECG signals. Via simple sewing methods, the conductive Ag-SBS fabric electrodes could be firmly integrated into a T shirt and then stably perform the ECG signal collection (Figure 5G). The ECG signals collected by the woven fabric electrodes showed high similarity to those collected by commercial ECG patches (Figure S5A), exhibiting high reliability of the Ag-SBS fabric in health-care monitoring applications. Most importantly, the conductive textiles showed outstanding washing ability. After 20 cycles of standard

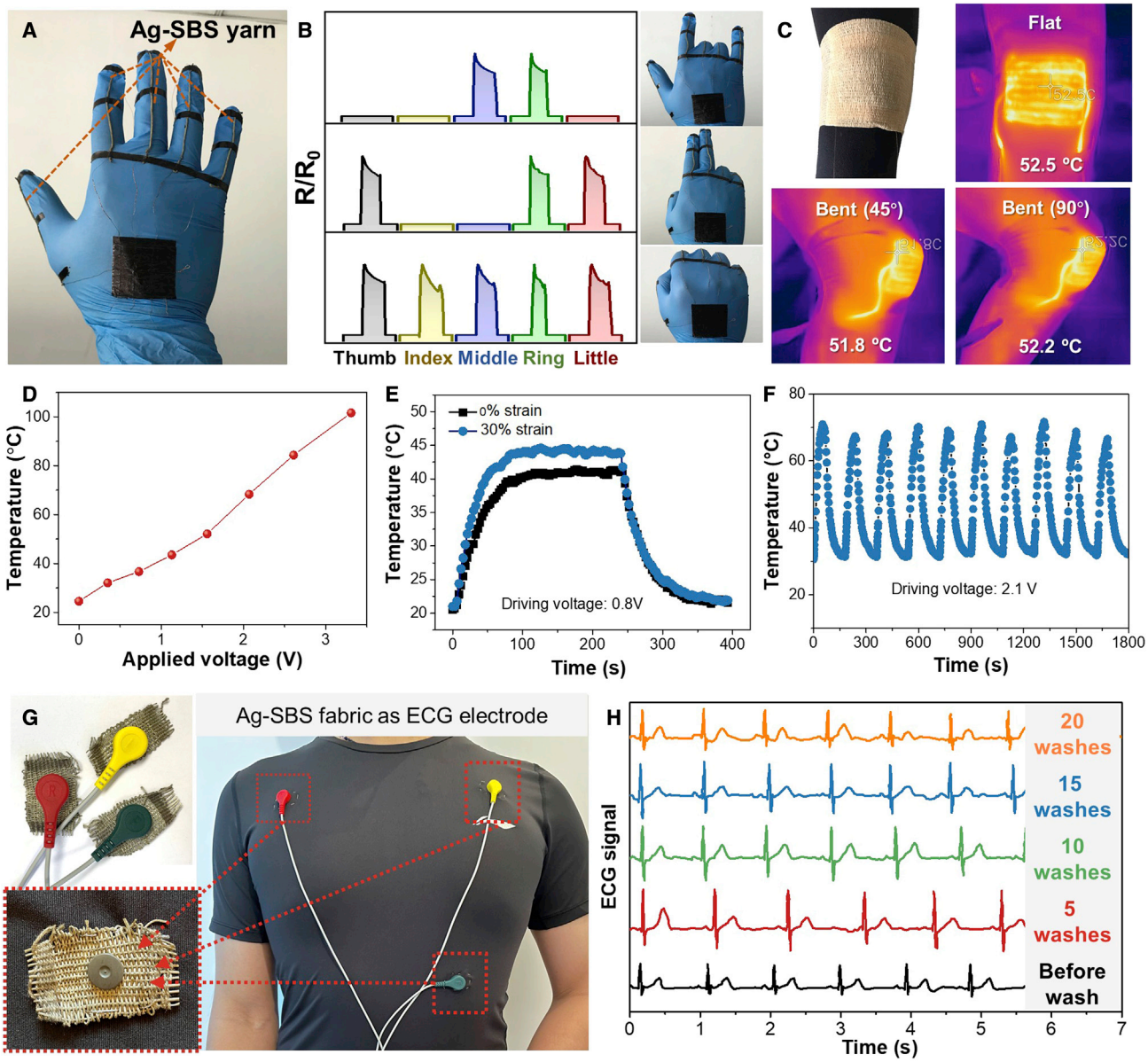

Figure 5. Applications of Ag-SBS textiles in wearable electronics

(A) Digital image showing the glove with integrated Ag-SBS yarn as a sensor to detect finger motion.

(B) Resistance change in the Ag-SBS yarn on the glove in response to different gestures of the fingers.

(C) Digital image showing an Ag-SBS fabric bandage worn on the knee and steadily performing heating function under bending conditions.

(D) Temperature changes in the Ag-SBS fabric as a function of driving voltage.

(E) Heating and cooling kinetics of the Ag-SBS fabric at relaxed and stretched (30% strain) states (driving voltage 0.8 V).

(F) Temperature change in the Ag-SBS fabric during cycling heating and cooling steps.

(G) Digital images showing three pieces of Ag-SBS fabric serving as electrodes and attaching onto a T shirt for ECG signal collection.

(H) ECG signals collected by the Ag-SBS fabric before and after repeated washes.

laundry washing, the resistance of the Ag-SBS increased by only ~16%, while the morphology of the Ag-SBS yarns remained unchanged (Figures S5B–S5D). Such Ag-SBS fabric electrodes were still able to stably collect the ECG signals without any obvious noise and distortion on the waveforms, further demonstrating the washing endurance of the Ag-SBS textiles (Figure 5H).

In summary, this work demonstrates, for the first time, a continuous fabrication strategy based on MMTD and chemical deposition processes that allows efficient and high-throughput fabrication of high-performance stretchable and conductive Ag-SBS monofilament and multifilament yarns in a roll-to-roll manner. The fiber and yarn parameters can be easily tuned to simultaneously reach high stretchability and high conductivity. Importantly, these one-dimensional fibers and yarns are strong and robust enough to be woven, knitted, or braided into smart textiles that can undergo standard machine washing. Such a seamless integration manner enables outstanding breathability and wearability of the wearable devices. We believe that this work provides an innovative fabrication option for developing stretchable fibers with various types of functionalities. Further exploration of the material combinations for fibers and the engineering of the fabrication processes could significantly enrich the materials library and thus greatly benefit the next-generation applications such as textile electronics, soft robotics, stretchable electronics, and biomechanical engineering.

EXPERIMENTAL PROCEDURES

Resource availability

Lead contact

Further information and requests for resources and reagents should be directed to and will be fulfilled by the lead contact, Prof. Zijian Zheng (tczzheng@polyu.edu.hk).

Materials availability

This study did not generate new unique reagents. All materials used in this study are available from the lead contact upon request.

Data and code availability

The data supporting the findings of this study are available from the lead contact upon request. This paper does not report original code.

Fabrication of Ag-SBS fibers

Ag-SBS fiber was prepared via an MMTD method followed by the loading of AgNPs in a roll-to-roll chemical deposition process. The fabrication processes could be summarized into four steps: (1) thermal drawing of core-shell structured PMMA@SBS fiber, (2) removal of the PMMA shell by soaking in acetic acid, (3) loading of AgNPs via chemical deposition, and (4) collection of fibers. First, an SBS rod (diameter 20 mm, length 85 mm) was inserted into a PMMA tube (diameter 30 mm, wall thickness 3 mm, length 125 mm) to form a core-cladding PMMA@SBS preform for the thermal drawing process. The preform was then thermally drawn into a continuous core-shell-structured PMMA@SBS fiber with a fiber-drawing tower, where the fiber-drawing temperature was set as ~250°C (heating rate ~1°C min^{-1}). During the fiber-drawing process, the preform was fed into the furnace at a speed of ~1 mm s^{-1}, while the drawing speed was tuned with a range of 3 to 80 mm s^{-1} to obtain the PMMA@SBS fibers with controllable diameter. Afterward, the as-drawn PMMA@SBS fiber was fed into a tank containing acetic acid, in which the PMMA core was completely dissolved. The tank was heated to 60°C to accelerate the dissolution of the PMMA core and the formation of SBS fiber. Subsequently, the SBS fiber was continuously fed into another tank with an ethanolic solution of AgTFA ($AgCF_3COO_2$, concentration ~17 wt %) for the loading of Ag precursor, followed by passing the Ag precursor-loaded SBS fiber into another tank with an ethanolic solution of hydrazine (10 vol %) to reduce the Ag ions and generate AgNPs on the SBS fiber. After being thoroughly rinsed with deionized water and drying at 60°C, the Ag-SBS fiber was eventually obtained and collected on a cone for the subsequent fabrication and

characterization. The loading amount of AgNPs could be further enhanced by repeating the loading of Ag precursors and the chemical reduction processes.

Fabrication of Ag-SBS multifilament yarns

To form an Ag-SBS multifilament yarn, the core-shell-structured PMMA@SBS fiber prepared in the above-mentioned process was cut into several sticks with a length of ~320 mm, which were then inserted into another PMMA tube (diameter 30 mm, wall thickness 3 mm, length 320 mm) to form a core-cladding PMMA@PMMA@SBS preform. Then the preform was thermally drawn into a continuous fiber (denoted as PMMA@PMMA@SBS fiber) under the same conditions as for preparing the PMMA@SBS fiber. Afterward, the PMMA shell of the PMMA@PMMA@SBS filament was removed by acetic acid, resulting in the formation of an SBS fiber bundle containing the designed number of SBS filaments. Subsequent loading of Ag precursors and chemical reduction processes were carried out to impart electrical conductivity to the as-prepared SBS multifilament. To introduce twists into the Ag-SBS multifilament, the preform was rotated at a controlled speed during the thermal drawing process.

Characterization

The morphology of the samples (PMMA@SBS preform and as-drawn fiber, SBS fiber, PMMA@PMMA@SBS fiber, SBS multifilament yarn, Ag-SBS fiber, Ag-SBS multifilament yarn) was investigated by SEM (Quanta 200; Hitachi). Mechanical properties of the samples (SBS fiber, Ag-SBS fiber, and Ag-SBS multifilament yarn) were investigated using an Instron 5566 universal testing system. Electrical and electromechanical properties of the Ag-SBS fibers were studied using a home-made setup containing a computer-controlled stretching machine and a Keithley 2400 source meter. The electrothermal performance of the Ag-SBS fabric was recorded by a Flir One Pro TG165 infrared camera. ECG signal collection using the Ag-SBS fabric as the electrode was performed using a Heal Force PC 80D ECG meter. The washability test for Ag-SBS fabrics was conducted by referring to AATCC Test Method 135. The T shirt sewn with three pieces of Ag-SBS fabric electrodes was put into a laundry bag and then loaded into a laundering machine (3LWTW4815FW0; Whirlpool). Additional cotton fabrics serving as the laundering ballast pieces were loaded to make a total weight of 1.8 kg fabrics for each washing. White washing mode, including washing, rinsing, and spinning, was selected to perform the machine laundering cycles. An entire laundering cycle lasted for around 50 min. The samples were removed from the machine and hung to dry in the air every five washing cycles for the evaluation of morphological and electrical changes.

SUPPLEMENTAL INFORMATION

Supplemental information can be found online at https://doi.org/10.1016/j.xcrp.2023.101300.

ACKNOWLEDGMENTS

We are grateful for financial support from the General Research Fund of Hong Kong (PolyU 153032/18), Hong Kong Scholars (XJ2016051), The Hong Kong Polytechnic University (1-ZVT8), and research project of Zhejiang Lab (113014-AC2101). Z.M. and Q.H. contributed equally to this work.

AUTHOR CONTRIBUTIONS

Z.Z. and Z.M. conceived and designed the experiments. Z.M. and N.Z. performed the experiments. Z.M., Q.H., Q.Z., and S.-W.N. performed the materials characterization. Z.M. and Q.H. analyzed the data and wrote the manuscript. Z.M., Q.H.,

and Z.Z. reviewed and edited the manuscript. Z.Z. supervised the project. All authors discussed the results and commented on the manuscript.

DECLARATION OF INTERESTS

The authors have a patent pending related to this work.

Received: November 23, 2022
Revised: January 3, 2023
Accepted: January 27, 2023
Published: February 21, 2023

REFERENCES

1. Chen, M., Wang, Z., Li, K., Wang, X., and Wei, L. (2021). Elastic and stretchable functional fibers: a review of materials, fabrication methods, and applications. Adv. Fiber Mater. *3*, 1–13. https://doi.org/10.1007/s42765-020-00057-5.

2. Matsuhisa, N., Chen, X., Bao, Z., and Someya, T. (2019). Materials and structural designs of stretchable conductors. Chem. Soc. Rev. *48*, 2946–2966. https://doi.org/10.1039/C8CS00814K.

3. Someya, T., and Amagai, M. (2019). Toward a new generation of smart skins. Nat. Biotechnol. *37*, 382–388. https://doi.org/10.1038/s41587-019-0079-1.

4. Ma, Z., Huang, Q., Xu, Q., Zhuang, Q., Zhao, X., Yang, Y., Qiu, H., Yang, Z., Wang, C., Chai, Y., et al. (2021). Permeable superelastic liquid-metal fibre mat enables biocompatible and monolithic stretchable electronics. Nat. Mater. *20*, 859–868. https://doi.org/10.1038/s41563-020-00902-3.

5. Lee, J., Llerena Zambrano, B., Woo, J., Yoon, K., and Lee, T. (2020). Recent advances in 1D stretchable electrodes and devices for textile and wearable electronics: materials, fabrications, and applications. Adv. Mater. *32*, 1902532. https://doi.org/10.1002/adma.201902532.

6. Wang, S., Xu, Q., and Sun, H. (2022). Functionalization of fiber devices: materials, preparations and applications. Adv. Fiber Mater. *4*, 324–341. https://doi.org/10.1007/s42765-021-00120-9.

7. Agcayazi, T., Chatterjee, K., Bozkurt, A., and Ghosh, T.K. (2018). Flexible interconnects for electronic textiles. Adv. Mater. Technol. *3*, 1700277. https://doi.org/10.1002/admt.201700277.

8. Huang, Q., and Zheng, Z. (2022). Pathway to developing permeable electronics. ACS Nano *16*, 15537–15544. https://doi.org/10.1021/acsnano.2c08091.

9. Shi, J., Liu, S., Zhang, L., Yang, B., Shu, L., Yang, Y., Ren, M., Wang, Y., Chen, J., Chen, W., et al. (2020). Smart textile-integrated microelectronic systems for wearable applications. Adv. Mater. *32*, 1901958. https://doi.org/10.1002/adma.201901958.

10. Chen, M., Li, P., Wang, R., Xiang, Y., Huang, Z., Yu, Q., He, M., Liu, J., Wang, J., Su, M., et al. (2022). Multifunctional fiber-enabled intelligent health agents. Adv. Mater. *34*, 2200985. https://doi.org/10.1002/adma.202200985.

11. Lee, J., Shin, S., Lee, S., Song, J., Kang, S., Han, H., Kim, S., Kim, S., Seo, J., Kim, D., et al. (2018). Highly sensitive multifilament fiber strain sensors with ultrabroad sensing range for textile electronics. ACS Nano *12*, 4259–4268. https://doi.org/10.1021/acsnano.7b07795.

12. Lee, J., Kwon, H., Seo, J., Shin, S., Koo, J.H., Pang, C., Son, S., Kim, J.H., Jang, Y.H., Kim, D.E., et al. (2015). Conductive fiber-based ultrasensitive textile pressure sensor for wearable electronics. Adv. Mater. *27*, 2433–2439. https://doi.org/10.1002/adma.201500009.

13. Liu, Z.F., Fang, S., Moura, F.A., Ding, J.N., Jiang, N., Di, J., Zhang, M., Lepró, X., Galvão, D.S., Haines, C.S., et al. (2015). Hierarchically buckled sheath-core fibers for superelastic electronics, sensors, and muscles. Science *349*, 400–404. https://doi.org/10.1126/science.aaa7952.

14. Toi, P.T., Trung, T.Q., Dang, T.M.L., Bae, C.W., and Lee, N.-E. (2019). Highly electrocatalytic, durable, and stretchable nanohybrid fiber for on-body sweat glucose detection. ACS Appl. Mater. Interfaces *11*, 10707–10717. https://doi.org/10.1021/acsami.8b20583.

15. Xu, Q., Liu, H., Zhong, X., Jiang, B., and Ma, Z. (2020). Permeable weldable elastic fiber conductors for wearable electronics. ACS Appl. Mater. Interfaces *12*, 36609–36619. https://doi.org/10.1021/acsami.0c08939.

16. Zamarayeva, A.M., Ostfeld, A.E., Wang, M., Duey, J.K., Deckman, I., Lechêne, B.P., Davies, G., Steingart, D.A., and Arias, A.C. (2017). Flexible and stretchable power sources for wearable electronics. Sci. Adv. *3*, e1602051. https://doi.org/10.1126/sciadv.1602051.

17. Pan, Z., Yang, J., Li, L., Gao, X., Kang, L., Zhang, Y., Zhang, Q., Kou, Z., Zhang, T., Wei, L., et al. (2020). All-in-one stretchable coaxial-fiber strain sensor integrated with high-performing supercapacitor. Energy Storage Mater. *25*, 124–130. https://doi.org/10.1016/j.ensm.2019.10.023.

18. Xiao, X., Xiao, X., Zhou, Y., Zhao, X., Chen, G., Liu, Z., Wang, Z., Lu, C., Hu, M., Nashalian, A., et al. (2021). An ultrathin rechargeable solid-state zinc ion fiber battery for electronic textiles. Sci. Adv. *7*, eabl3742. https://doi.org/10.1126/sciadv.abl3742.

19. Xiong, T., He, B., Zhou, T., Wang, Z., Wang, Z., Xin, J., Zhang, H., Zhou, X., Liu, Y., and Wei, L. (2022). Stretchable fiber-shaped aqueous aluminum ion batteries. EcoMat *4*, e12218. https://doi.org/10.1002/eom2.12218.

20. Guan, X., Xu, B., Huang, J., Jing, T., and Gao, Y. (2022). Fiber-shaped stretchable triboelectric nanogenerator with a novel synergistic structure of opposite Poisson's ratios. Chem. Eng. J. *427*, 131698. https://doi.org/10.1016/j.cej.2021.131698.

21. Zhang, C., Zhang, Q., Zhang, D., Wang, M., Bo, Y., Fan, X., Li, F., Liang, J., Huang, Y., Ma, R., and Chen, Y. (2021). Highly stretchable carbon nanotubes/polymer thermoelectric fibers. Nano Lett. *21*, 1047–1055. https://doi.org/10.1021/acs.nanolett.0c04252.

22. Mokhtari, F., Spinks, G.M., Sayyar, S., Cheng, Z., Ruhparwar, A., and Foroughi, J. (2021). Highly stretchable self-powered wearable electrical energy generator and sensors. Adv. Mater. Technol. *6*, 2000841. https://doi.org/10.1002/admt.202000841.

23. Yang, Z., Deng, J., Sun, X., Li, H., and Peng, H. (2014). Stretchable, wearable dye-sensitized solar cells. Adv. Mater. *26*, 2643–2647,2613. https://doi.org/10.1002/adma.201400152.

24. Zhang, Z., Yang, Z., Deng, J., Zhang, Y., Guan, G., and Peng, H. (2015). Stretchable polymer solar cell fibers. Small *11*, 675–680. https://doi.org/10.1002/smll.201400874.

25. Chen, F., Huang, Q., and Zheng, Z. (2022). Permeable conductors for wearable and on-skin electronics. Small Struct. *3*, 2100135. https://doi.org/10.1002/sstr.202100135.

26. Li, X., Hu, H., Hua, T., Xu, B., and Jiang, S. (2018). Wearable strain sensing textile based on one-dimensional stretchable and weavable yarn sensors. Nano Res. *11*, 5799–5811. https://doi.org/10.1007/s12274-018-2043-7.

27. Wang, Z., Huang, Y., Sun, J., Huang, Y., Hu, H., Jiang, R., Gai, W., Li, G., and Zhi, C. (2016). Polyurethane/cotton/carbon nanotubes core-spun yarn as high reliability stretchable strain sensor for human motion detection. ACS Appl. Mater. Interfaces *8*, 24837–24843. https://doi.org/10.1021/acsami.6b08207.

28. Yang, Z., Wang, W., Bi, L., Chen, L., Wang, G., Chen, G., Ye, C., and Pan, J. (2020). Wearable electronics for heating and sensing based on a multifunctional pet/silver nanowire/PDMS yarn. Nanoscale *12*, 16562–16569. https://doi.org/10.1039/D0NR04023A.

29. Zu, M., Li, Q., Wang, G., Byun, J.-H., and Chou, T.-W. (2013). Carbon nanotube fiber based

stretchable conductor. Adv. Funct. Mater. *23*, 789–793. https://doi.org/10.1002/adfm.201202174.

30. Xu, Z., Liu, Z., Sun, H., and Gao, C. (2013). Highly electrically conductive Ag-doped graphene fibers as stretchable conductors. Adv. Mater. *25*, 3249–3253. https://doi.org/10.1002/adma.201300774.

31. Shang, Y., He, X., Li, Y., Zhang, L., Li, Z., Ji, C., Shi, E., Li, P., Zhu, K., Peng, Q., et al. (2012). Super-stretchable spring-like carbon nanotube ropes. Adv. Mater. *24*, 2896–2900. https://doi.org/10.1002/adma.201200576.

32. Son, W., Chun, S., Lee, J.M., Lee, Y., Park, J., Suh, D., Lee, D.W., Jung, H., Kim, Y.-J., Kim, Y., et al. (2019). Highly twisted supercoils for superelastic multi-functional fibres. Nat. Commun. *10*, 426. https://doi.org/10.1038/s41467-018-08016-w.

33. Zhu, S., So, J.H., Mays, R., Desai, S., Barnes, W.R., Pourdeyhimi, B., and Dickey, M.D. (2013). Ultrastretchable fibers with metallic conductivity using a liquid metal alloy core. Adv. Funct. Mater. *23*, 2308–2314. https://doi.org/10.1002/adfm.201202405.

34. Leber, A., Dong, C., Chandran, R., Das Gupta, T., Bartolomei, N., and Sorin, F. (2020). Soft and stretchable liquid metal transmission lines as distributed probes of multimodal deformations. Nat. Electron. *3*, 316–326. https://doi.org/10.1038/s41928-020-0415-y.

35. Chen, S., Liu, H., Liu, S., Wang, P., Zeng, S., Sun, L., and Liu, L. (2018). Transparent and waterproof ionic liquid-based fibers for highly durable multifunctional sensors and strain-insensitive stretchable conductors. ACS Appl. Mater. Interfaces *10*, 4305–4314. https://doi.org/10.1021/acsami.7b17790.

36. Lee, S., Shin, S., Lee, S., Seo, J., Lee, J., Son, S., Cho, H.J., Algadi, H., Al-Sayari, S., Kim, D.E., and Lee, T. (2015). Ag nanowire reinforced highly stretchable conductive fibers for wearable electronics. Adv. Funct. Mater. *25*, 3114–3121. https://doi.org/10.1002/adfm.201500628.

37. Seyedin, S., Uzun, S., Levitt, A., Anasori, B., Dion, G., Gogotsi, Y., and Razal, J.M. (2020). Mxene composite and coaxial fibers with high stretchability and conductivity for wearable strain sensing textiles. Adv. Funct. Mater. *30*, 1910504. https://doi.org/10.1002/adfm.201910504.

38. Li, W., Zhou, Y., Wang, Y., Li, Y., Jiang, L., Ma, J., and Chen, S. (2020). Highly stretchable and sensitive sbs/graphene composite fiber for strain sensors. Macromol. Mater. Eng. *305*, 1900736. https://doi.org/10.1002/mame.201900736.

39. Qu, Y., Nguyen-Dang, T., Page, A.G., Yan, W., Das Gupta, T., Rotaru, G.M., Rossi, R.M., Favrod, V.D., Bartolomei, N., and Sorin, F. (2018). Superelastic multimaterial electronic and photonic fibers and devices via thermal drawing. Adv. Mater. *30*, 1707251. https://doi.org/10.1002/adma.201707251.

40. Tao, G., Stolyarov, A.M., and Abouraddy, A.F. (2012). Multimaterial fibers. Int. J. Appl. Glass Sci. *3*, 349–368. https://doi.org/10.1111/ijag.12007.

41. Kaufman, J.J., Tao, G., Shabahang, S., Deng, D.S., Fink, Y., and Abouraddy, A.F. (2011). Thermal drawing of high-density macroscopic arrays of well-ordered sub-5-nm-diameter nanowires. Nano Lett. *11*, 4768–4773. https://doi.org/10.1021/nl202583g.

42. Zou, Y., Liu, C., Ren, Z., Zhang, Y., Liu, Z., Xu, Y., Hou, C., Yang, L., Liang, S., and Tao, G. (2022). Flexible and robust low-loss selenium-based multimaterial infrared fibers towards CO_2 laser ablation. iScience *25*, 105167. https://doi.org/10.1016/j.isci.2022.105167.

43. Yan, W., Dong, C., Xiang, Y., Jiang, S., Leber, A., Loke, G., Xu, W., Hou, C., Zhou, S., Chen, M., et al. (2020). Thermally drawn advanced functional fibers: new frontier of flexible electronics. Mater. Today *35*, 168–194. https://doi.org/10.1016/j.mattod.2019.11.006.

44. Loke, G., Yan, W., Khudiyev, T., Noel, G., and Fink, Y. (2020). Recent progress and perspectives of thermally drawn multimaterial fiber electronics. Adv. Mater. *32*, 1904911. https://doi.org/10.1002/adma.201904911.

45. Chen, M., Wang, Z., Zhang, Q., Wang, Z., Liu, W., Chen, M., and Wei, L. (2021). Self-powered multifunctional sensing based on super-elastic fibers by soluble-core thermal drawing. Nat. Commun. *12*, 1416. https://doi.org/10.1038/s41467-021-21729-9.

46. Dong, C., Leber, A., Das Gupta, T., Chandran, R., Volpi, M., Qu, Y., Nguyen-Dang, T., Bartolomei, N., Yan, W., and Sorin, F. (2020). High-efficiency super-elastic liquid metal based triboelectric fibers and textiles. Nat. Commun. *11*, 3537. https://doi.org/10.1038/s41467-020-17345-8.

47. Zhang, Y., Li, X., Kim, J., Tong, Y., Thompson, E.G., Jiang, S., Feng, Z., Yu, L., Wang, J., Ha, D.S., et al. (2021). Thermally drawn stretchable electrical and optical fiber sensors for multimodal extreme deformation sensing. Adv. Opt. Mater. *9*, 2001815. https://doi.org/10.1002/adom.202001815.

48. Lu, C., Park, S., Richner, T.J., Derry, A., Brown, I., Hou, C., Rao, S., Kang, J., Mortiz, C.T., Fink, Y., and Anikeeva, P. (2017). Flexible and stretchable nanowire-coated fibers for optoelectronic probing of spinal cord circuits. Sci. Adv. *3*, e1600955. https://doi.org/10.1126/sciadv.1600955.

49. Wang, D., Zhang, Y., Lu, X., Ma, Z., Xie, C., and Zheng, Z. (2018). Chemical Formation of soft metal electrodes for flexible and wearable electronics. Chem. Soc. Rev. *47*, 4611–4641. https://doi.org/10.1039/c7cs00192d.

50. Li, P., Zhang, Y., and Zheng, Z. (2019). Polymer-assisted metal deposition (PAMD) for flexible and wearable electronics: principle, materials, printing, and devices. Adv. Mater. *31*, 1902987. https://doi.org/10.1002/adma.201902987.

51. Rao, C., and Trivedi, D. (2005). Chemical and electrochemical depositions of platinum group metals and their applications. Coord. Chem. Rev. *249*, 613–631. https://doi.org/10.1016/j.ccr.2004.08.015.

52. Park, M., Im, J., Shin, M., Min, Y., Park, J., Cho, H., Park, S., Shim, M.B., Jeon, S., Chung, D.Y., et al. (2012). Highly stretchable electric circuits from a composite material of silver nanoparticles and elastomeric fibres. Nat. Nanotechnol. *7*, 803–809. https://doi.org/10.1038/nnano.2012.206.

53. Horev, Y.D., Maity, A., Zheng, Y., Milyutin, Y., Khatib, M., Yuan, M., Suckeveriene, R.Y., Tang, N., Wu, W., and Haick, H. (2021). Stretchable and highly permeable nanofibrous sensors for detecting complex human body motion. Adv. Mater. *33*, 2102488. https://doi.org/10.1002/adma.202102488.

54. Youn, C., Gwak, H.J., Bae, Y., Kim, D., Yeang, B.J., Doh, S.J., and Yeo, S.Y. (2022). Improving mechanical properties of melt-spun polyetherimide monofilaments by thermal drawing. J. Appl. Polym. Sci. *139*, e53155. https://doi.org/10.1002/app.53155.

55. Goto, S., Kirchheim, R., Al-Kassab, T., and Borchers, C. (2007). Application of cold drawn lamellar microstructure for developing ultra-high strength wires. Trans. Nonferrous Met. Soc. China *17*, 1129–1138. https://doi.org/10.1016/S1003-6326(07)60238-6.

56. Liao, X., Dulle, M., de Souza e Silva, J.M., Wehrspohn, R.B., Agarwal, S., Förster, S., Hou, H., Smith, P., and Greiner, A. (2019). High strength in combination with high toughness in robust and sustainable polymeric materials. Science *366*, 1376–1379. https://doi.org/10.1126/science.aay9033.

57. Xiang, X., Yang, Z., Di, J., Zhang, W., Li, R., Kang, L., Zhang, Y., Zhang, H., and Li, Q. (2017). In situ twisting for stabilizing and toughening conductive graphene yarns. Nanoscale *9*, 11523–11529. https://doi.org/10.1039/C7NR03305B.

58. Seyedin, S., Moradi, S., Singh, C., and Razal, J.M. (2018). Continuous production of stretchable conductive multifilaments in kilometer scale enables facile knitting of wearable strain sensing textiles. Appl. Mater. Today *11*, 255–263. https://doi.org/10.1016/j.apmt.2018.02.012.